Implementation of a Morse potential to model hydroxyl behavior in phyllosilicates

Jeffery A. Greathouse,[a] Justin S. Durkin, James P. Larentzos, and Randall T. Cygan
Geochemistry Department, Sandia National Laboratories, Albuquerque, New Mexico 87185-0754, USA

(Received 23 December 2008; accepted 27 February 2009; published online 7 April 2009)

The accurate molecular simulation of many hydrated chemical systems, including clay minerals and other phyllosilicates and their interfaces with aqueous solutions, requires improved classical force field potentials to better describe structure and vibrational behavior. Classical and *ab initio* molecular dynamics simulations of the bulk structure of pyrophyllite, talc, and Na-montmorillonite clay phases exhibit dissimilar behavior in the hydroxyl stretch region of power spectra derived from atomic trajectories. The classical simulations, using the CLAYFF force field, include either a standard harmonic potential or a new Morse potential parametrized for both dioctahedral and trioctahedral phases for the O–H bond stretch. Comparisons of classical results with experimental values and with *ab initio* molecular dynamics simulations indicate improvements in the simulation of hydroxyl orientation relative to the clay octahedral sheet and in the O–H bond stretch in the high frequency region of the power spectrum. © *2009 American Institute of Physics*. [DOI: 10.1063/1.3103886]

I. INTRODUCTION

Clay minerals are of significant interest in many chemical, geological, materials, medical, catalysis, and related industrial applications.[1,2] Comprised of two-dimensional sheets and layers, phyllosilicates include a wide variety of multicomponent low-symmetry clay minerals having variable layer charge. Layer charge is an important characteristic of these phases and ranges from no charge with van der Waals forces controlling the interactions between layers to low charge clay phases such as smectites that can readily expand with water or other intercalates, to relatively high-charge phases such as muscovite and other micas having strong electrostatic forces act between layers. Outside of a few exceptions, clay minerals typically occur as nanoparticles although they are conventionally defined by a grain size of less than 2 μm.[1] Despite the technological benefits that nanoparticles provide, the limited grain size of clay minerals prevents an accurate interrogation of crystal structure—especially for the characterization of hydroxyls and water—by most analytical methods. In recent years, however, molecular simulations of clay mineral systems have proven to be an extraordinarily useful supplement to x-ray diffraction, vibrational spectroscopy, and other conventional analytical methods.[3] Furthermore, recent advances in sophisticated software and high-end multiprocessor computing, and the availability of accurate clay force fields, have brought increased fidelity to the simulation of clay phases.[4]

In general, phyllosilicates are two-dimensional periodic layered minerals consisting of an octahedrally coordinated metal-oxide sheet sandwiched between two tetrahedrally coordinated silicate sheets (2:1 structures). The structural and vibrational properties of the endmember uncharged dioctahedral (pyrophyllite) and trioctahedral (talc) phases were previously investigated using classical and *ab initio* molecular dynamics (AIMD) simulations.[5] This effort also evaluated the accuracy of using the flexible force field CLAYFF (Ref. 6) to predict structures and vibrational spectra. Pyrophyllite ($Al_2Si_4O_{10}(OH)_2$) and talc ($Mg_3Si_4O_{10}(OH)_2$) have different octahedral sheets and exhibit dissimilar dispositions of the hydroxyl groups. The molecular simulation results[5] for these uncharged clay minerals suggest that although structural models are relatively accurate, additional refinement of the force field parameters is required to properly describe the O–H bond length and improve dynamical behavior of hydroxyl groups. In general, the hydroxyl group behavior of clay minerals is fundamental to our understanding of many interfacial and adsorption processes, but it is difficult to ascertain these details through spectroscopy.

Electronic structure calculations based on density functional theory (DFT) have been used to examine the role of site substitution and hydroxyl orientation in dioctahedral phases[7,8] and the dynamics of hydroxyl groups based on composition and substitution within tetrahedral and octahedral sheets.[5,9] Recently, Churakov[10,11] examined the structure and dynamics of hydroxyl groups associated with the edges sites of pyrophyllite using Car–Parrinello molecular dynamics (MD). Collectively, these theoretical studies have provided significant detailed insights into how the hydroxyl chemistry of clay minerals is controlled by clay composition and structure. However, for many clay mineral applications involving interfacial phenomena, basal and edge surface adsorption, intercalation, and other complex processes, it is critical to have a classical force field that accurately describes hydroxyl behavior, especially for large many-atom systems that prohibit the use of costly DFT methods.

In this study, we refine a widely used classical force field to more accurately reproduce the structural and vibrational behaviors of layer hydroxyl groups in 2:1 layered clay minerals. In addition to pyrophyllite and talc, we extend these

[a]Electronic mail: jagreat@sandia.gov. Tel.: (505) 284-4895. FAX: (505) 844-7354.

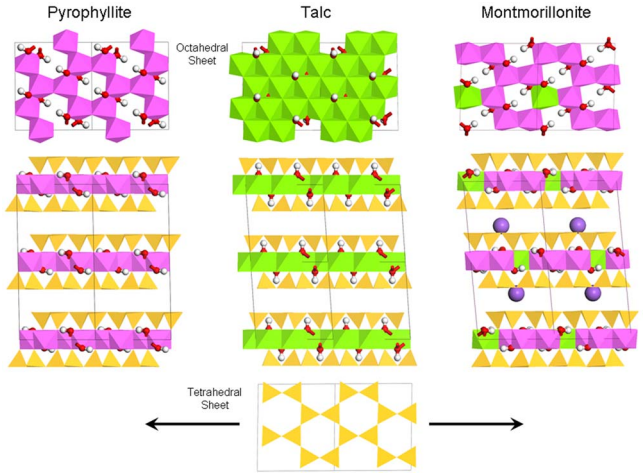

FIG. 1. (Color online) Polyhedron models of the structures of pyrophyllite (left), talc (center), and Na-montmorillonite (right) with views normal to the basal surface (top and bottom) showing the octahedral and tetrahedral sheets (talc only), and as viewed along the *a*-axis to emphasize the layers (center). Hydroxyl groups are highlighted as ball and stick representations and Na^+ ions are indicated as gray (purple) spheres in the montmorillonite interlayer. Aluminum and magnesium coordinations are represented by dark gray (pink) and gray (green) octahedra, respectively; silicon tetrahedra are noted by light gray (yellow) polyhedra.

techniques to examine the common soil mineral montmorillonite, a charged 2:1 layered clay mineral. Substitution of magnesium for aluminum within the octahedral sheet creates negatively charged layers with a structural composition of $Na_x(Mg_xAl_{1-x})Si_2O_5(OH)$, where $0<x<1$ (see Fig. 1). In this notation, x refers to the layer charge, defined as the number of mole net electron charge per unit cell that is produced by isomorphic substitution.[12] To facilitate the negatively charged clay layers, monovalent and/or divalent cations are located within the interlayer and are amenable to ion exchange. Additionally, the presence of counterbalancing ions within the interlayers increases the hydrophilic nature of these minerals. Results from AIMD simulations are compared with those from classical models using the modified CLAYFF force field with particular attention to the vibrational behavior quantified in power spectra. Finally, we present a discussion of model accuracy based on these comparisons and the use of a Morse potential for the hydroxyl bond in clay minerals.

II. COMPUTATIONAL METHODS

A. DFT

To construct the model structure of montmorillonite, a related dioctahedral phyllosilicate, muscovite $(KAl_2(Si_3Al)O_{10}(OH)_2)$, was used as a template.[13] The muscovite crystal structure is well defined crystallographically, with lattice constants $a=5.1765$ Å, $b=8.9872$ Å, $c=20.072$ Å, $\alpha=\beta=90.0°$, $\gamma=95.756°$, and a $2M_1$ polytype. The muscovite unit cell consists of two layers, where the layer registry shift is appropriate for modeling montmorillonite. The muscovite unit cell was expanded to create a $2\times1\times1$ supercell, and the compositions of the tetrahedral and octahedral sheets were adjusted to reflect the appropriate montmorillonite formula, $Na_2(Mg_2Al_{14})(Si_2O_5)_{16}(OH)_{16}$. Sodium cations are incorporated in the interlayer to balance the negative charge of the layers created by the octahedral substitution of magnesium for aluminum. Vacancies in the octahedral sheet were distributed in an ordered pattern at the $M1$ sites. Hydroxyl groups are located along the $M1$ mirror plane and adjacent to the vacancies. The disposition of the hydroxyl groups is highly dependent on the local structure within the tetrahedral and octahedral sheets, but has a large impact on the adsorption and ion exchange characteristics of the mineral.

To validate the suitability of the model structure, the *d*-spacing and lattice constants of Na-montmorillonite were computed using DFT. Periodic plane-wave DFT calculations were performed with the Vienna *ab initio* simulation package (VASP).[14,15] Frozen-core electronic states were described using the accurate projector-augmented wave approach,[16,17] electron exchange and correlation were treated within the generalized gradient approximation according to Perdew–Wang,[18] and plane waves were included to a 400 eV energy cutoff. Because of the sufficiently large simulation cells, the Brillouin-zone sampling was restricted to the Γ point.

Canonical ensemble (constant *NVT*, N=number of atoms, V=volume, T=temperature) AIMD simulations were conducted with the montmorillonite model while providing full translational symmetry ($P1$ symmetry). After 12 ps of equilibration at 300 K, statistics were collected every 2 fs during a 20 ps production run. The velocity Verlet algorithm was used to update positions every time step, $\Delta t=0.5$ fs. To reduce the energy drift to 1 K ps^{-1}, the energy convergence tolerance for the electronic self-consistency loop at each Born–Oppenheimer step was set to 10^{-7} eV.[19] While we previously employed *NVE* (E=total potential energy) simulations to obtain power spectra for talc and pyrophyllite,[5] the thermodynamic convergence criteria were not satisfactory for montmorillonite even at a small timestep of 0.25 fs. We therefore chose the *NVT* ensemble to ensure thermodynamic equilibrium at the longer timestep of 0.5 fs. This technique has been used successfully on AIMD simulations of similar clay systems.[20,21] Atomic velocities were used in vibrational analysis for both AIMD and classical MD simulations, as described in the next section.

B. Classical simulations

For the classical simulations, a nonbonded force field (CLAYFF) was used to describe all atomic interactions except for the hydroxyl group, which requires a bond stretch term.[6] The nonbond potential energy E_{nonbond} between two atoms i and j separated by a distance r consists of electrostatic and Lennard-Jones terms, given by

$$E_{\text{nonbond}}=\frac{q_iq_j}{4\pi\varepsilon_0 r}+4\varepsilon_{ij}\left[\left(\frac{\sigma_{ij}}{r}\right)^{12}-\left(\frac{\sigma_{ij}}{r}\right)^{6}\right], \quad (1)$$

where q_i and q_j are atomic charges, ε_0 is the dielectric permittivity of vacuum, ε_{ij} represents the potential well depth for Lennard-Jones attraction, and σ_{ij} is the Lennard-Jones diameter of the atomic pair. Combination rules are used when $i\neq j$, such that $\varepsilon_{ij}=(\varepsilon_i\varepsilon_j)^{1/2}$ and $\sigma_{ij}=1/2(\sigma_i$

TABLE I. Nonbonded force field parameters.

Element	Atom type	q/e	ε (kcal mol^{-1})	σ (Å)
Octahedral Al	ao	1.5750	1.3298×10^{-6}	4.2713
Si	st	2.1000	1.8405×10^{-6}	3.3020
Mg	mgo	1.3600	9.0298×10^{-7}	5.2643
Tetrahedral O in Si–O–Si	ob	−1.0500	0.1554	3.1655
Octahedral O in (SiAlMg)O	obos	−1.1808	0.1554	3.1655
Octahedral O in (SiMgMg)O	obss	−1.2996	0.1554	3.1655
O(H) in AlAl(OH)	oh	−0.9500	0.1554	3.1655
O(H) in AlMg(OH)	ohs	−1.0808	0.1554	3.1655
H(O)	ho	0.4250	0.0000	0.0000
Na	Na	1.0000	0.1301	2.3500

$+\sigma_j$).[22] Potential parameters for nonbonded interactions according to Eq. (1) are given in Table I.

Initially, as developed, a harmonic potential was used in CLAYFF to describe the bond energy E_{harmonic} between O and H atoms separated by a distance r,

$$E_{\text{harmonic}} = k(r - r_0)^2, \tag{2}$$

where r_0 is the equilibrium bond distance and k represents the bond strength. In this work we also consider the Morse potential for O–H bond interactions,

$$E_{\text{Morse}} = D_0[1 - e^{-\alpha(r-r_0)}]^2, \tag{3}$$

where α is related to the width of the potential energy curve and D_0 is the depth of the potential well. Potential parameters for O–H bonded interactions according to Eqs. (2) and (3) are given in Table II. The Morse parameters given in Table II are specific to the type of clay (octahedral versus tetrahedral), and the procedure to optimize those parameters is discussed below.

MD simulations were performed with the LAMMPS code[23] using the statistical *NVE* ensemble. Short-range interactions were evaluated every 0.5 fs with a real-space cutoff of 10.0 Å, and long-range electrostatics interactions were evaluated every 1.0 fs using an efficient particle-particle particle-mesh summation algorithm[24] with a precision of 1.0×10^{-4}. After an equilibration stage of 250 ps, a production stage (1000 ps) was used for structural analysis with a data collection frequency of 0.5 ps. An additional 40 ps MD stage was used to obtain atomic trajectories for subsequent vibrational analysis using the TINKER software.[25] The velocity autocorrelation function (VACF) for each atom type was obtained as follows:

TABLE II. Bonded parameters for O and H atoms.

	Harmonic [Eq. (2)]		Morse [Eq. (3)]		
Clay type	k (kcal mol^{-1} Å^{-2})	r_0 (Å)	D_0 (kcal mol^{-1})	α (Å^{-1})	r_0 (Å^{-1})
Dioctahedral	553.935	1.0000	132.2491	2.1815	0.9450
Trioctahedral	553.935	1.0000	132.2491	2.1350	0.9572

$$C(t) = \frac{1}{N}\sum_{j=1}^{N}[v_j(0)\cdot v_j(t)], \tag{4}$$

which sums the dot product of atomic velocity $v_j(t)$ relative to an initial velocity $v_j(0)$. The summation in Eq. (4) incorporates the number of atoms of a given atom type or the entire set of atoms for a total VACF. The frequency-based power spectrum was calculated by squaring the Fourier-transformed VACF. Sampling every 2.0 fs in Eq. (4) ensured that vibrational frequencies up to 8000 cm^{-1} were captured, and a windowing gap of 6.0 ps was used to give a frequency resolution of approximately 2.8 cm^{-1}. Separate VACF and power spectra were obtained for each atom type and for an "all atom" power spectrum.

The simulation systems consisted of two neutral clays (pyrophyllite and talc) and one negatively charged clay (Na-montmorillonite). In each case, orthorhombic unit cells were created from triclinic cells[6] and then expanded into supercells. Table III reviews the composition of each clay supercell. The two neutral clays were simulated previously,[5] but the simulations were repeated but now using a Morse potential to represent the O–H bond stretch. All three clay phases contain a two-dimensional periodic layer consisting of octahedrally coordinated atoms (Mg or Al) sandwiched between two tetrahedrally coordinated silicate sheets, as shown in Fig. 1. Pyrophyllite and Na-montmorillonite are referred to as dioctahedral clays because of the three available octahedral metal sites only two are occupied by aluminum atoms. The vacancy is located in the $M1$ octahedral site. The negative charge in montmorillonite arises due to isomorphic substitution of magnesium for aluminum in the octahedral sheet, which is balanced by interlayer sodium ions. In contrast, talc is a trioctahedral clay having all three octahedral metal sites occupied by magnesium ions.

C. Optimization of the Morse potential parameters for O–H bonds

The Morse parameters were optimized with a series of classical geometry minimizations and normal mode analysis using the Discover module of MATERIALS STUDIO software

TABLE III. Supercell composition for classical MD simulations.

Clay mineral	Unit cell formula	Supercell size (Å^3)	No. atoms
Pyrophyllite	$Al_2(Si_4O_{10})(OH)_2$	$41.7\times35.9\times28.0$	3840
Talc	$Mg_3(Si_4O_{10})(OH)_2$	$42.3\times36.7\times27.4$	4032
Na-montmorillonite	$Na_{0.75}(Al_{3.25}Mg_{0.75})(Si_8O_{20})(OH)_4$	$36.0\times41.4\times37.3$	5184

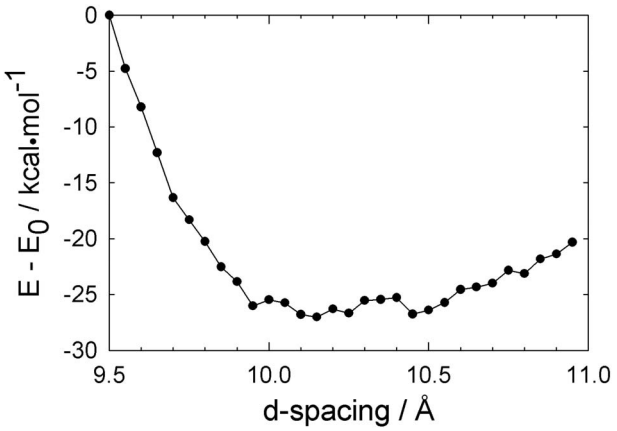

FIG. 2. Energy profile for Na-montmorillonite obtained from constant-volume DFT geometry optimizations. The plotted energies (e) are shown relative to a reference energy at a *d*-spacing of 9.5 Å (E_0).

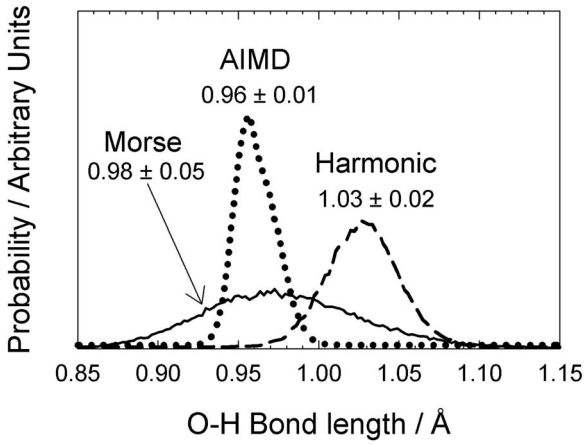

FIG. 3. O–H bond length distributions for Na-montmorillonite obtained from classical MD (Morse and harmonic bond stretch potentials) and AIMD simulations. The average bond length and standard deviation are indicated next to each distribution curve.

(Accelrys Inc., San Diego). This procedure was performed separately for uncharged trioctahedral (talc) and dioctahedral (pyrophyllite) clay phases. Smaller supercell sizes were used for the energy minimizations: $21.16\times18.346\times18.92$ and $20.64\times17.932\times18.694$ Å^3 for talc and pyrophyllite, respectively. All system cells were in orthorhombic configurations. The initial Morse parameters were taken from a gas-phase water model, whose parameters were optimized for the vibrational properties of water.[26] First, the r_0 parameter was adjusted until the geometry-optimized O–H bond length matched the results obtained from DFT calculations.[5] Second, the α parameter was adjusted until the O–H stretch frequency ($\approx$3700 cm^{-1}) from normal mode analysis matched the experimental frequencies.[27] Finally, the optimized Morse parameters were confirmed using MD simulations of the larger supercells described in Table III. The D_0 parameter was left unmodified due to the satisfactory results obtained by only varying α and r_0. Also, D_0 is equivalent to the O–H dissociation energy of the water model and is well known. The optimized Morse parameters are given in Table II.

III. RESULTS AND DISCUSSIONS

A. DFT geometry optimization of Na-montmorillonite

The crystallographic *c*-parameter of Na-montmorillonite was systematically varied from 19.0 to 21.9 Å in increments of 0.1 Å, while ensuring a uniform interlayer spacing. Constant-volume geometry optimizations were performed, allowing full translational symmetry (*P*1 symmetry) of the atoms while constraining the supercell lattice values. For dehydrated Na-montmorillonite, the minimum potential energy was observed at *d*-spacing values—equivalent to repeat distance of basal planes—between 9.95 and 10.25 Å as shown in Fig. 2. This is in good agreement with the experimental value of 9.6 Å obtained by x-ray diffraction.[1] Overall, the DFT pseudopotentials provide an adequate description of the structural properties of Na-montmorillonite. The optimized structure obtained at a *d*-spacing of 10.15 Å was used as the model input structure for subsequent AIMD simulations. The O–H bond length in the optimized structure is 0.965 Å. We define the orientation angle of the O–H group with respect to the (001) plane as ρ, which for the optimized structure is 2.4°. The interlayer sodium ions are located at the midplane of the interlayer, but not directly above or below the octahedral (magnesium) charge sites. The Na–Mg distances for one of the sodium interlayer ions are 5.4 and 6.7 Å, while for the other interlayer the distances are 6.5 and 6.9 Å.

B. MD simulations at 300 K

Results from classical MD simulation are compared with those from AIMD simulations for uncharged clays (pyrophyllite and talc) and a negatively charged clay (Na-montmorillonite). Classical simulations were performed using both the harmonic and Morse potentials for the O–H bond stretch, and the resulting O–H bond length distributions for montmorillonite are shown in Fig. 3. The Morse potential results in much better agreement with the more rigorous AIMD method than those obtained using the harmonic potential, although the Morse distribution of O–H bond lengths is significantly wider. This wider distribution indicates that higher bond stretch energies are sampled with the Morse potential compared to the harmonic potential. Using Eqs. (2) and (3), we calculated the bond energies at the bond distance standard deviation limits for both potentials. The maximum bond energy sampled with the Morse potential is approximately three times higher than with the harmonic potential. A similar trend is seen for the uncharged clays (pyrophyllite and talc), where the average O–H bond lengths using the Morse potential are 0.97 ± 0.04 and 0.99 ± 0.04 Å, respectively.

The use of the Morse potential in the classical simulations has little effect on other structural properties for the clay layer hydroxyl, as shown in Table IV. The Al–O–H and Mg–O–H angles are mainly controlled by nonbond interactions between Al–O and Mg–O pairs, which are not affected by the Morse O–H potential. The Morse potential results in a slight improvement over the harmonic potential (relative to the DFT results) in the hydroxyl orientation with respect to the (001) plane (ρ). For dioctahedral clays such as pyrophyl-

TABLE IV. Average values (deg) for M–O–H angles (M=Al or Mg) and orientation ρ of OH with respect to the (001).

		Pyrophyllite	Talc	Montmorillonite
M–O–H angle	CLAYFF-harmonic	119 ± 12	123 ± 9	115 ± 14
	CLAYFF-Morse	120 ± 11	123 ± 3	116 ± 14
	AIMD	122 ± 7	121 ± 8	117 ± 8
ρ angle	CLAYFF-harmonic	15 ± 21	79 ± 6	5 ± 22
	CLAYFF-Morse	18 ± 20	79 ± 6	7 ± 21
	AIMD	28 ± 16	80 ± 5	17 ± 17

lite and montmorillonite, the hydroxyl group lies nearly parallel to the (001) plane, but for trioctahedral clays such as talc, the fully occupied octahedral sheet forces the hydroxyl group to be nearly perpendicular to the (001) plane. The results in Table IV are consistent with this description. The case of dioctahedral clays is a much more challenging problem for classical simulations because of the existence of the $M1$ vacancies. The hydroxyl orientation is influenced by the octahedral charge centers (Mg substitutions) as well as hydrogen bond interactions between hydrogen atoms and siloxane oxygen atoms. Although hydrogen bonding is not explicitly included in the energy expression, it is implicit in the combined interactions of electrostatics, van der Waals, and the new Morse potential. In all three simulations, ρ is smaller in montmorillonite than pyrophyllite. In montmorillonite, layer oxygen atoms coordinated to octahedral magnesium atoms (obos and obss atom types, Table I) are more negatively charged than the other layer oxygen atoms (ob atom type, Table I). We believe that the resulting increase in electrostatic attraction between hydrogen atoms and the more negative oxygen atoms controls the decrease in ρ as noted in Table IV. We also observe that the Morse potential used in classical simulations results in ρ values that are much smaller compared with AIMD structures. It is likely that a three-body angle bend term for Al–O–H or Mg–O–H groups will ultimately be needed in CLAYFF to overcome the structural disagreement.

An analysis of the vibrational motions from MD simulations is a powerful technique to validate the analytical functions and energy parameters in classical force fields. The calculated power spectra can be compared with vibrational spectra from infrared, Raman, or inelastic neutron scattering experiments. Power spectra do not incorporate molecular dipole or polarizability effects, so peak intensities cannot be directly compared with experimental spectra. However, for force field validation, the frequency of vibrational modes can be directly compared with experiment. Accurate prediction of vibrational spectra through simulation is challenging because the vibrational force constants are related to the second derivative of the potential energy function. Additionally, comparisons between classical MD and AIMD yield useful information regarding parameter development for classical force fields. We have previously analyzed the power spectra from MD simulations of pyrophyllite and talc.[5] The classical results using CLAYFF compared reasonably well with both AIMD and experimental spectra for many lattice modes, including Si–O stretch, tetrahedral SiO_4 bends, and Mg vibrations. However, the harmonic potential used to model the O–H stretch motion in the classical simulations resulted in a frequency that is too high and invariant to the local hydroxyl environment (see Fig. 4). Using the Morse potential for the O–H bond stretch with the parameters we derived for dioctahedral and trioctahedral clay minerals, we see much better agreement with the presumably more accurate AIMD results. However, the Morse peaks are much broader compared to either the AIMD or harmonic peaks, a feature which is probably related to the broader distribution in O–H bond length observed in Fig. 3. AIMD peaks are narrow due to the re-

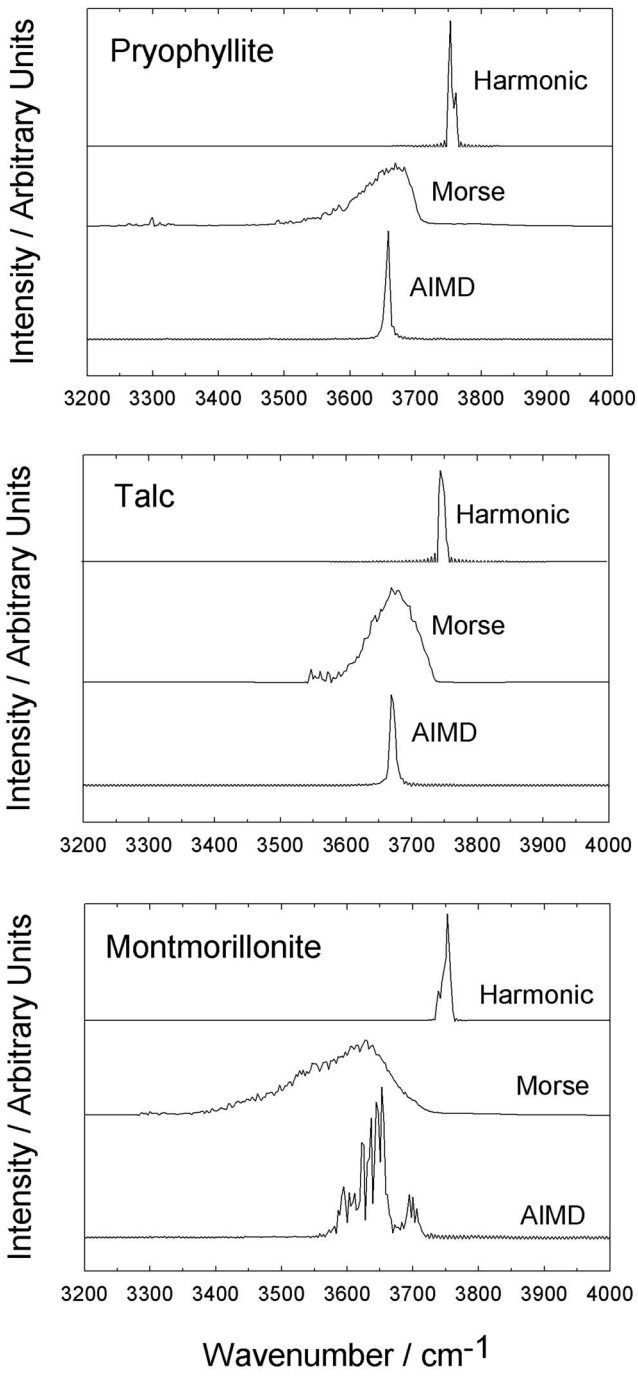

FIG. 4. Power spectra (H atoms only) corresponding to the O–H stretch motion for pyrophyllite, talc, and Na-montmorillonite in the region of 3200–4000 cm^{-1}. Results are shown from both classical MD simulations (Morse and harmonic bond stretch potentials) and AIMD.

strictive size of the simulation cell compared to classical MD. Additionally, the Morse potential successfully predicts the decrease in O–H stretch frequency between pyrophyllite (3670 cm^{-1}) and montmorillonite (3625 cm^{-1}), in agreement with AIMD. Using the harmonic potential, the O–H stretch frequency is similar in pyrophyllite and montmorillonite. The Morse parameters for O–H bond stretch given in Table II augment the transferability of CLAYFF potentials to other mineral systems, particularly those with surface hydroxyl groups.

While it is tempting to adjust the α value to reduce the peak broadening observed in Figs. 3 and 4, the agreement in O–H stretch frequency would be lost. We optimized the Morse r_0 and α values based on structural (O–H bond length) and energetic (O–H stretch frequency) considerations, respectively. Parameter selection was based on static energy calculations, so peak broadening due to statistical or thermal effects could not be considered. The broad peaks seen in Fig. 4 with the Morse potential are almost certainly related to the higher bond energies sampled compared to the harmonic potential, as discussed previously. As a result, the Morse potential is more sensitive to changes in the local molecular environment, which is critical for transferability of these parameters to new model systems. Our long-term goal is to apply the Morse potential to systems that contain surface hydroxyl groups, where the asymmetry about the equilibrium bond distance provided by the Morse potential will be preferred over the symmetric harmonic potential. Finally, we note that the O–H stretch peak is widest for montmorillonite compared to the uncharged endmember clays. The presence of octahedral magnesium atoms in the clay is accompanied by charge redistribution among surrounding atoms and the presence of charge-balancing sodium ions in the interlayer. The Morse potential is more responsive to this structural disorder, while the harmonic potential is insensitive to changes in the local molecular environment.

Another interesting feature in Fig. 4 is the observed split in the O–H stretch band in the AIMD spectrum for Na-montmorillonite. This effect is not observed when using the Morse potential in the classical MD simulations due to peak broadening, but we also note that the AIMD peak is much broader than the corresponding peak in pyrophyllite. Depending on the hydroxyl orientation in the *ab* plane, different hydrogen bonding interactions with nearby clay oxygen atoms could lead to the observed peak splitting. Because this split is not observed in the AIMD spectrum for pyrophyllite, we conclude that the effect is due to magnesium charge sites in montmorillonite.

In addition to hydrogen atoms, other atomic power spectra aid in comparisons between CLAYFF and AIMD simulations, and with experiment. Figure 5 contains atomic power spectra of Na-montmorillonite for both AIMD and CLAYFF (Morse) simulations, and key frequencies are given in Table V. The assignment of vibrational modes was aided by animation of the results of a normal mode analysis. The frequency range of Si–O modes (as noted by the power spectra for the st and ob atom types in Fig. 5) is in good agreement with experiment. We observe that CLAYFF slightly overpredicts these frequencies, as was the case in pyrophyllite and talc.[5] The O–H in-plane deformation mode observed experimentally at 915 cm^{-1} for pyrophyllite[27] is a consequence of the steric freedom of the layer hydroxyl in response to the presence of octahedral vacancies. For montmorillonite, an additional O–H deformation peak at lower frequency is observed in the experimental spectra (Table V). In the simulated power spectra, this second peak cannot be unambiguously assigned, although the AIMD peak at 820 cm^{-1} could be due to O–H deformation. Even with the Morse potential for O–H bond interactions, the CLAYFF frequency for the O–H in-plane deformation mode (820 cm^{-1}) is nearly 100 cm^{-1} lower than AIMD or experiment results. The same situation was observed in the pyrophyllite spectra.[5] This discrepancy is further evidence that a three-body M–O–H term is probably needed for the accurate simulation of dioctahedral clays. Both CLAYFF and AIMD agree with experiment on the higher frequency tetrahedral SiO_4 mode and the octahedral AlO_6 mode, and reasonable agreement is observed for the low-frequency mode assigned to translation of sodium ions within the clay interlayer.

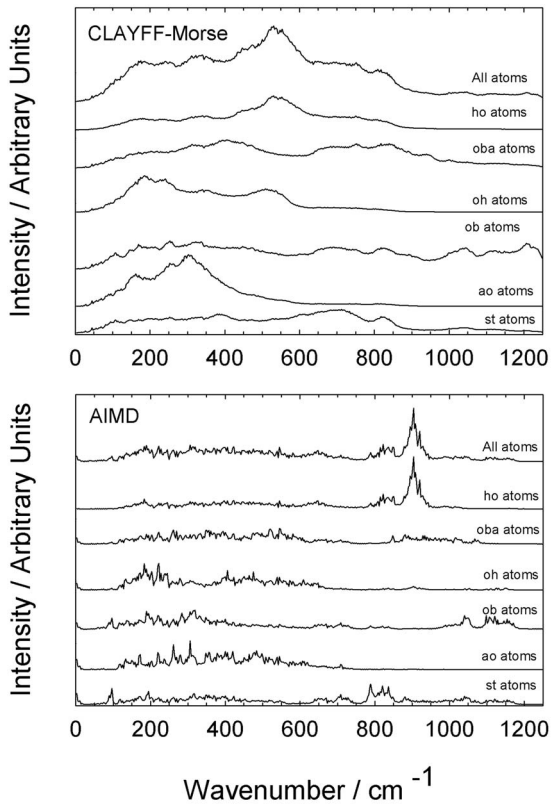

FIG. 5. Power spectra for Na-montmorillonite in the low-frequency region. Results are shown from both classical MD simulations (Morse bond stretch potential) and AIMD. The atom-type designations are described in Table I. Individual spectra were scaled in intensity for ease of viewing.

IV. CONCLUSIONS

Accurate classical models of the hydroxyl bond in complex phases such as clay minerals are critical to the analysis of structure and dynamics of many hydrated chemical systems, especially in our understanding of interfacial and adsorption behavior where hydroxyls and water play a key role. Given the shortcoming of conventional experimental and

TABLE V. Vibrational frequencies (cm^{-1}) for Na-montmorillonite obtained from atomic power spectra.

Mode	Simulation			Experiment	
	CLAYFF (this work)	AIMD (this work)	DFT normal mode analysis[a]	Raman[b]	FTIR
O–H stretch	3625	3650	3675–3708		3630[c]
Si–O stretch	1035, 1120, 1215	990, 1040, 1125		1135	1021–1115[d]
O–H deformation, in-plane	820	905	732–874	798, 915	842, 916[c]
O–H deformation, out of plane	530	650	452–623		
Raman SiO_4 bend (a_1)	700	710		440, 480, 725	
AlO_6 octahedra	180	180		173, 190	
Interlayer Na^+ vibration	200, 125	60		89	

[a]Data from Botella *et al.* (Ref. 9). Vibrational modes were reported for pyrophyllite, in which all hydroxyl oxygen atoms are bonded to two aluminum atoms (designated AlAlOH), and a Na-smectite with 50% each AlAlOH and AlMgOH hydroxyl linkages. Note that in our model we have 25% AlMgOH and 75% AlAlOH.
[b]Raman spectrum of Chambers Na-montmorillonite (mostly octahedral substitution) (Ref. 28).
[c]Fourier transform infrared (FTIR) spectra of dehydrated Na-montmorillonite designated as Na-SAz-1, which contains only octahedral substitution (Ref. 29).
[d]FTIR spectra of dehydrated Na-montmorillonite designated as Na-SWy-1 which contains both octahedral and tetrahedral substitutions (Ref. 30).

analytical methods to clearly ascertain key structural features and hydroxyl-related processes, it is important to more accurately refine our molecular simulations with improved force fields. The incorporation of a Morse potential in CLAYFF to better describe the hydroxyl bond stretch has significantly improved simulations of various endmember clay minerals including the uncharged pyrophyllite and talc and the charged Na-montmorillonite phase. We have parametrized the Morse potential to better mimic the O–H stretch mode observed in experiment and in our AIMD simulations for each of the three clay phases. The Morse potential accurately describes the vibrational frequency for the dioctahedral and trioctahedral phases, but is somewhat broadened compared to results using the previous CLAYFF harmonic potential and from our AIMD power spectra. Further modifications to CLAYFF or other classical force fields for the simulation of hydrated systems will necessarily require improvements to better model the relatively complex behavior of hydroxyl groups in layered minerals. This is no simple task as the simulation of vibrational spectra with classical force fields requires an accurate and robust description based on the second spatial derivative of the potential energy expression.

ACKNOWLEDGMENTS

We recognize support from the U.S. Department of Energy, Office of Basic Energy Sciences, Geosciences Research. Sandia is a multiprogram laboratory operated by Sandia Corporation, a Lockheed Martin company, for the U.S. Department of Energy under Contract No. DE-AC04-94AL85000.

[1] G. W. Brindley and G. Brown, *Crystal Structures of Clay Minerals and Their X-Ray Identification* (Mineralogical Society, London, 1980).
[2] S. W. Bailey, Rev. Mineral. **19**, 1 (1988).
[3] R. T. Cygan, J. A. Greathouse, H. Heinz, and A. G. Kalinichev, "Molecular models and simulations of layered materials," J. Mater. Chem. (unpublished).
[4] H. C. Greenwell, W. Jones, P. V. Coveney, and S. Stackhouse, J. Mater. Chem. **16**, 708 (2006).
[5] J. P. Larentzos, J. A. Greathouse, and R. T. Cygan, J. Phys. Chem. C **111**, 12752 (2007).
[6] R. T. Cygan, J.-J. Liang, and A. G. Kalinichev, J. Phys. Chem. B **108**, 1255 (2004).
[7] V. Timon, G. I. Sainz-Diaz, V. Botella, and A. Hernandez-Laguna, Am. Mineral. **88**, 1788 (2003).
[8] D. Tunega, B. A. Goodman, G. Haberhauer, T. G. Reichenauer, M. H. Gerzabek, and H. Lischka, Clays Clay Miner. **55**, 220 (2007).
[9] V. Botella, V. Timon, E. Escamilla-Roa, A. Hernandez-Languna, and C. I. Sainz-Diaz, Phys. Chem. Miner. **31**, 475 (2004).
[10] S. V. Churakov, Geochim. Cosmochim. Acta **71**, 1130 (2007).
[11] S. V. Churakov, J. Phys. Chem. B **110**, 4135 (2006).
[12] G. Sposito, *The Surface Chemistry of Soils* (Oxford University Press, New York, 1984).
[13] J. J. Liang, F. C. Hawthorne, and I. P. Swainson, Can. Mineral. **36**, 1017 (1998).
[14] G. Kresse and J. Furthmuller, Phys. Rev. B **54**, 11169 (1996).
[15] G. Kresse and J. Furthmuller, Comput. Mater. Sci. **6**, 15 (1996).
[16] P. E. Blochl, Phys. Rev. B **50**, 17953 (1994).
[17] G. Kresse and D. Joubert, Phys. Rev. B **59**, 1758 (1999).
[18] J. P. Perdew and Y. Wang, Phys. Rev. B **45**, 13244 (1992).
[19] D. Asthagiri, L. R. Pratt, and J. D. Kress, Phys. Rev. E **68**, 041505 (2003).
[20] D. Tunega, M. H. Gerzabek, G. Haberhauer, and H. Lischka, Eur. J. Soil Sci. **58**, 680 (2007).
[21] D. Tunega, G. Haberkauer, M. H. Gerzabek, and H. Lischka, Soil Sci. **169**, 44 (2004).
[22] T. A. Halgren, J. Am. Chem. Soc. **114**, 7827 (1992).
[23] S. J. Plimpton, J. Comput. Phys. **117**, 1 (1995).
[24] S. J. Plimpton, R. Pollock, and M. Stevens, Eighth SIAM Conference on Parallel Processing for Scientific Computing, 1997 (unpublished).
[25] TINKER, software tools for molecular design, Version 4.2 (http://dasher.wustl.edu/tinker/) (2004).
[26] J. R. Reimers and R. O. Watts, Mol. Phys. **52**, 357 (1984).
[27] V. C. Farmer, in *The Infrared Spectra of Minerals*, edited by V. C. Farmer (Mineralogical Society, London, 1974), p. 331.
[28] R. L. Frost and L. Rintoul, Appl. Clay Sci. **11**, 171 (1996).
[29] W. Z. Xu, C. T. Johnston, P. Parker, and S. F. Agnew, Clays Clay Miner. **48**, 120 (2000).
[30] C. T. Johnston and G. S. Premachandra, Langmuir **17**, 3712 (2001).